THE PENNSYLVANIA STATE UNIVERSITY

SCHREYER HONORS COLLEGE

DEPARTMENT OF MECHANICAL AND NUCLEAR ENGINEERING

MEASURING NORMALIZED DIFFERENCE VEGETATION INDEX FOR AGRICULTURAL MANAGEMENT USING UNMANNED AERIAL VEHICLES

CONNOR SCOTT DISCO

SPRING 2016

A thesis submitted in partial fulfillment of the requirements

for a baccalaureate degree in Mechanical Engineering

with honors in Mechanical Engineering

Reviewed and approved* by the following:

Henry Joseph Sommer III
Professor of Mechanical Engineering
Thesis Supervisor

Zoubeida Ounaies
Professor of Mechanical Engineering
Honors Adviser

* Signatures are on file in the Schreyer Honors College.

ABSTRACT

Healthy vegetation appears green because plant leaves reflect green light. Photosynthetic pigments in the leaves also reflect near infrared (NIR) light, with healthier pigments reflecting the highest amount of NIR light. Accordingly, by measuring a plant's NIR reflectivity, it is possible to assess its health visually. The Normalized Differential Vegetation Index (NDVI) is a measurement of the amount of NIR light reflected from a plant's leaves and has been used as an assessment of plant health for various agricultural applications. The use of NDVI for health analysis is important to the agricultural community but the specialized cameras currently used to measure NDVI are much too expensive to make implementation of NDVI analysis widely accessible. As such, this research serves three purposes: to mimic the NDVI image-capturing process using less-expensive digital cameras, to develop unmanned aerial platforms which can easily be implemented by small-scale agriculturalists to perform aerial NDVI analysis, and to develop software to post-process images and provide an NDVI color map of the area of land analyzed. Developing an inexpensive and easy-to-use platform allows agriculturalists to affordably implement NDVI analysis to manage plant health and could revolutionize the agricultural industry as a whole.

TABLE OF CONTENTS

LIST OF FIGURES

LIST OF TABLES

ACKNOWLEDGEMENTS

I wish to express my deepest gratitude to all those who helped make this research possible. I would like to thank the Schreyer Honors College for providing the scholarship funding to support my education and for the wealth of staff who have assisted me every step of the way. I also owe great appreciation to Dr. Sommer for his guidance over the course of my research efforts. Without his patience and willingness to share both his time and knowledge, none of this work would have been possible. I would also like to thank all those we interacted with in the Agricultural Department and at the Larson Agricultural Center for their help in coordination with my research efforts. Lastly, I would like to thank all my friends and family who supported me throughout this process.

Chapter 1 Introduction

Recent developments in technology have afforded society the opportunity to advance the methods with which it performs activities throughout life. These advancements range from those that impact society as a whole, such as improving travel with the development of cleaner and more-efficient vehicles, to those that simply make life for individuals more enjoyable, such as improvements in the newest smart phone or virtual reality device. One recent advancement that has crossed the barrier between utility and pleasure is the increase in availability of unmanned aerial vehicles (UAVs) to the public. UAVs with increasingly advanced technology including flight planning using GPS and high definition live video streaming have become more affordable and thus more widely used. Some analysts compare drone development of the 2010's to the development of PC's in the 1990's pointing out the parallels between them. Both sectors began with a small number of companies developing new technology followed later by a larger number of competitors. While PC's began with IBM and Apple, UAV development has begun with companies like DJI and 3DR. Both sectors also began with a hobbyist market and then exploded into the commercial sector. A writer for Drone Life predicts, "if drones follow the PC pricing-decrease model, we can expect, for example, to see the DJI Phantom 3 Advanced to move from its current price point of $999 to $879 by next year and down to $525 by 2020" [1]. With the price of consumer UAVs dropping steadily, they are becoming more viable not just for use by the casual hobbyist, but also for implementation in industry. Amazon, for example, is investigating the use of UAVs in their delivery service. Many of the packages delivered by Amazon are under five pounds, which makes the use of UAVs for short-range deliveries a potential. While there are still

logistical issues associated with the concept including approval from the Federal Aviation Association (FAA), Amazon is fully devoting resources to study the feasibility of implementing package-delivering UAVs [2]. UAVs have also begun to be utilized for safety and rescue. DJI's vice president of policy and legal affairs stated to CNBC that, "there are countless applications for using drones to help people. One the most beneficial is search and rescue" [3]. Compared to the high operating cost of a helicopter, which can run into thousands of dollars per hour, emergency responders have been utilizing relatively inexpensive UAVs equipped with specialized cameras and sensors to spot people day or night. Responders then use this information to identify where a helicopter or ground crew would need to be dispatched. Additionally, law enforcement agencies see potential uses for UAVs in HAZMAT operations, traffic accidents, and bomb disposal to name a few [3]. Seeing how impactful UAVs could be in these areas, investigating the feasibility of using UAVs in other industries could yield promising results. With this in mind, the following research examines the possibility of capturing the utility of UAVs for use in maintaining agricultural health.

Background

In order to be able to use UAVs to study plant health, it is first important to understand what makes a plant healthy, beginning with knowledge of the photosynthetic process. Photosynthesis occurs as plants absorb energy from light. This process is inherently dependent on the energy of the light itself and thus photosynthesis is wavelength-dependent. The energy of a photon is inversely proportionate to the wavelength as shown in the Equation 1 on the following page where E denotes energy, c the speed of light, λ wavelength, and h Planck's constant [4].

$$E = \frac{h * c}{\lambda} \qquad \text{[Eq. 1]}$$

Visible light consists of a range of wavelengths shown in Figure 1 ranging from low blue (380 nm) to far-red light (750 nm). The region between 400 nm and 700 nm shown below is the range used by plants to drive photosynthesis and is referred to as Photosynthetically Active Radiation (PAR) [5]. The inverse relationship shown in Equation 1 indicates that low range PAR such as blue light consists of high-energy photons while high range red light is much lower energy.

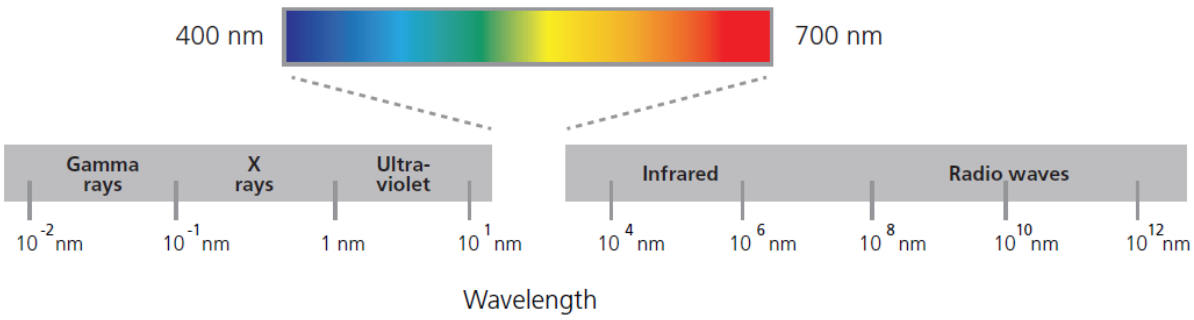

Figure 1 Visible Spectrum of Light [5]

In relation to photosynthesis, there are two important spectrums of visible light: the absorption spectra, which defines the wavelengths of light that are absorbed by a plant, and the action spectrum, which defines the wavelengths that are most effective for photosynthesis [5]. Photosynthesis is driven by pigments in the leaves of plants, which allow for the absorption of light. The most important is Chlorophyll-a as shown in Figure 2 which depicts both the rate of photosynthesis and the absorption due to Chlorophyll-a as a function of wavelength in the visible spectrum[6].

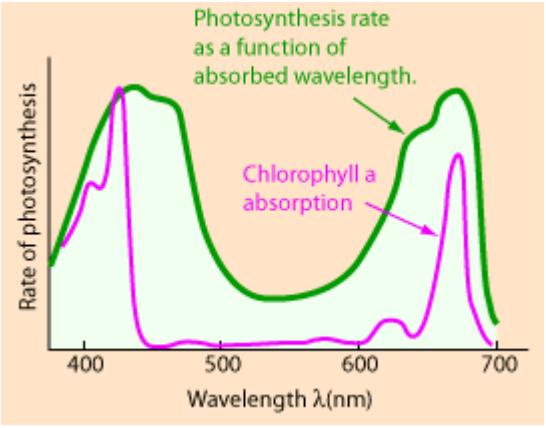

Figure 2 Rate of Photosynthesis as a Function of Wavelength [6]

While photosynthesis is most strongly influenced by Chlorophyll-a, it is also a function of the absorption rate of Chlorophyll-b and accessory pigments called carotenoids. All three of these pigments have peak absorption rates in the high-energy blue and low-energy red ranges as shown in Figure 3. Consequently, the absorption spectra for plants consists mainly of these ranges. This is why LED lamps used for growing plants typically consist of blue and red LED lights [5].

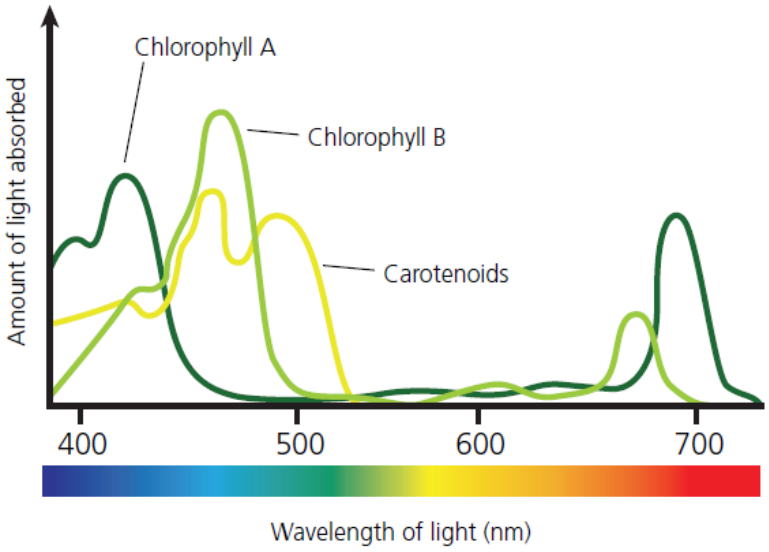

Figure 3 Absorption Spectrum of Visible Light [5]

The action spectrum further categorizes the ranges of absorbed light by the efficiency with which each produces a photochemical reaction, thus effectively defining which wavelengths actually drive photosynthesis. An article published by McCree in 1972 studied the action spectrum of twenty-two plant species [5]. This study used the quantum yield of carbon dioxide as the metric for efficiency and interestingly found similar spectrums for all twenty-two plants, showing only slightly more variation in the blue range. Nevertheless, this study showed that the areas of spectrum that most strongly drive photosynthesis are in the red region (600-700nm) followed by the blue region (400-500nm). The lowest-yield region, as could be predicted from Figure 2 and Figure 3, was green light (500-600nm).

This evidence confirms that the healthiest vegetation absorbs a high amount of red light and reflects green, hence why healthy vegetation appears green to the naked eye. Further work has been done to examine how light just outside the visible range could be a similar indicator of plant health. Specifically, scientists have looked at how plants reflect near infrared (NIR) light, in the region of approximately 850nm just above the red region of the spectrum. Studies have shown that, similar to how plants performing photosynthesis most-effectively reflect green light, a high level of NIR reflectivity is indicative of healthy vegetation [7]. This is because healthy leaves have a spongy layer found on their bottom surface, which strongly reflects NIR light. When a plant becomes dehydrated, its leaves reflect less light in the NIR range of the light spectrum as this spongy layer decreases. The relationship between health and NIR as well as the relationship between NIR and the other main color bands of the visible spectrum is illustrated on the following page in Figure 4 [7].

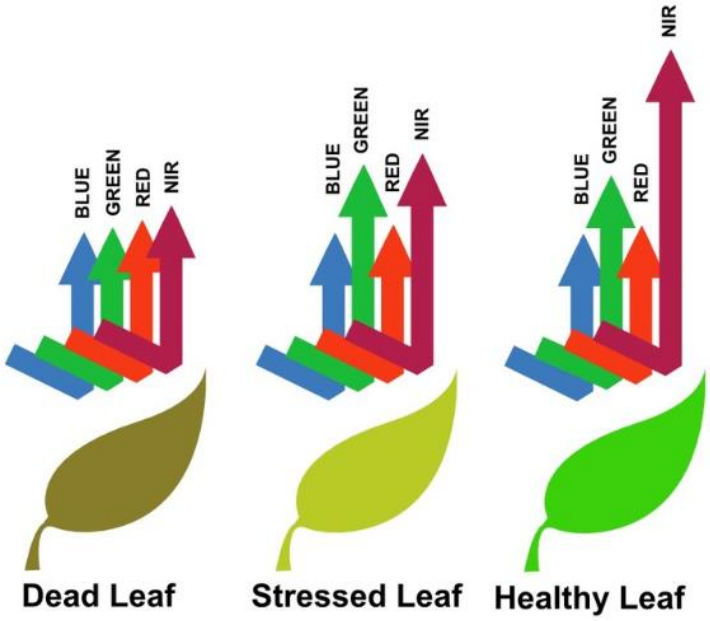

Figure 4 Relationship Between Leaf Health and Light Reflectivity [7]

The relationship between NIR and red band reflectivity proves to be extremely useful in the evaluation of plant health by enabling researchers to study optical data of vegetation. While healthy leaves reflect NIR light but not red light, soil reflects both. Consequently, by taking an overhead picture and comparing the difference between NIR light reflected and red light reflected, researchers can differentiate between healthy vegetation, stressed or dead vegetation, and the soil beneath the vegetation. This led researchers to begin utilizing a metric known as Normalized Difference Vegetation Index (NDVI) to evaluate vegetation which is expressed in Equation 2 below [7].

$$\mathrm{NDVI} = \frac{\mathrm{NIR} - \mathrm{red}}{\mathrm{NIR} + \mathrm{red}} \qquad \text{[Eq. 2]}$$

The potential application of such a development is both wide-ranging and extremely impactful. While NDVI analysis has been implemented through satellite image collection,

capitalizing on the ever-increasing utility of small-scale UAVs to perform similar analysis could enable everyday agriculturalists to perform scientific studies of their vegetation with relative ease. Consequently, this thesis seeks to examine both the hardware and software developments that would be necessary to construct a platform for small-scale NDVI vegetation analysis. The successful development of such a system could have immense impact on the agricultural industry affecting applications ranging from the analysis of the health of many types of crops, to the detection of parasitic plant growth such as vines that could kill a crop, to the management of turf grass on golf courses. This would allow more individuals who work with vegetation to utilize advanced technology at a relatively low cost and could revolutionize the industry. This paper will explore the feasibility of making such a revolution possible.

Chapter 2 Measuring Normalized Difference Vegetation Index (NDVI)

Utilization of the Normalized Difference Vegetation Index (NDVI) for the analytical study of plant health has the possibility to be relevant to a wide range of agricultural applications. It would provide scientific and objective formulae for the categorization of plant health, which could greatly influence the ability of agricultural professionals of effectively care for their crops. For instance, one of the major issues that can plague a crop is pests, which can sicken or kill a plant. The Food and Agriculture Organization (FAO) of the United Nations offers resources, which recommend steps to take to avoid pest infestation such as crop rotation, utilization of adequate cultivation techniques, and maintenance of field sanitation and hygiene among others [8]. In the event of pests infiltrating a crop, early detection is extremely important and the FAO works to educate farmers, stating that, "at farm level the farmers should also be aware of what different pests and beneficial organisms look like and what (if there is any) the tolerable level is in the field" [8]. Potential issues arise, however, in that the process of monitoring plants in this way is inherently subjective as well as requiring constant oversight. While this might be sustainable on smaller farms, this issue grows as scale increases. If farmers had an objective method of monitoring plant health, management could be performed more uniformly. If developed in an aerial system, utilizing NDVI would provide this standardized method of analysis as well as expedite the process of monitoring a large crop. Unfortunately, in order to measure infrared light to be used in the precise calculation of NDVI, special cameras are necessary which are expensive. There are three main categories of NDVI sensors: satellite, close-range, and aerial. Each of these will be discussed in the following sections.

Satellite Sensors

The Department of the Interior, NASA, and the Department of Agriculture have been monitoring the surface of the Earth via satellite images since July 23, 1972, the date the Earth Resources Technology Satellite (ERTS-1), which was later renamed Landsat 1, was launched into orbit [9]. This was the first of a series of satellites launched in the Landsat Program, which endeavored to study the Earth, examine changes over time, and to inventory and manage the Earth's resources. The Landsat 1 satellite carried a camera called the Return Beam Vidicon (RBV) which was meant to be the primary instrument, and a Multispectral Scanner (MSS). Although not originally predicted, the MSS data proved to be of higher quality [10]. The MSS utilized four spectral bands: two in the visible spectrum, green and red, and two infrared bands. These bands are shown below in Table 1 [11]. The MSS was used in subsequent missions and designations varied from Landsat 1-3 to Landsat 4-5.

Table 1 MSS Spectral Band Definition [11]

Landsat 1-3	Landsat 4-5	Wavelength (nm)	Resolution (m)
Band 4	Band 1	500-600	60
Band 5	Band 2	600-700	60
Band 6	Band 3	700-800	60
Band 7	Band 4	800-1100	60

The first three Landsat missions each carried the RBV and MSS sensors. Starting with Landsat 4, which was operational from 1982-1993, a Thematic Mapper (TM) was used which added three more bands including midrange infrared. The number of bands and range of

wavelength slowly expanded eventually reaching 11 bands in the Operational Land Imager (OLI) and Thermal Infrared Sensor (TIRS) equipped on the Landsat 8 satellite. These bands are defined in Table 2 [11]. Landsat 8 was launched in February 2013 and is still in orbit today. Landsat 9 is scheduled to launch in 2023.

Table 2 OLI and TIRS Band Definition [11]

Bands	Wavelength (nm)	Resolution (m)
Band 1- Coastal Aerosol	430-450	30
Band 2- Blue	450-510	30
Band 3- Green	530-590	30
Band 4- Red	640-670	30
Band 5 – Near Infrared	850-880	30
Band 6- SWIR 1	1,570-1,650	30
Band 7- SWIR 2	2,110-2,290	30
Band 8- Panchromatic	500-680	15
Band 9- Cirrus	1,360-1,380	30
Band 10 Thermal Infrared	10,600-11,190	30
Band 11- Thermal Infrared	11,500-12,510	30

The Landsat satellites have been able to provide extremely valuable data utilizing not only the visible spectrum, but also wavelengths outside what can be seen by the human eye. While having a large effect on human health, natural disaster relief, and energy for instance, the Landsat satellites have perhaps had the greatest effect on agriculture. Land surface covers approximately

thirty percent of the Earth's surface. Of this, about forty percent is devoted to agriculture [10]. Satellite imagery has allowed agricultural organizations "to analyze the health and vigor of crops as they mature over the growing season; the needs of specific fields for fertilizer, irrigation and rotation; planted acreage to forecast crop production and fight crop insurance fraud; how much water is used in irrigation; and the impacts of drought" [10]. Much of this information has been made possible from the use of non-visible spectral analysis such as thermal and NDVI. Shown in Figure 5 is an evapotranspiration (ET) map of the Colorado River Basin generated with one of the infrared bands of the satellite [10]. ET is water that transpires from plants that subsequently evaporates from the ground below and can be used to study water consumption. The blue areas in the image show areas that consume the most water, while the orange show areas with very little ET such as desert land. This type of image processing has allowed water managers to gather data not obtainable in the visible spectrum, study much larger areas at a time than previously possible, and examine trends over time with repeated image collection.

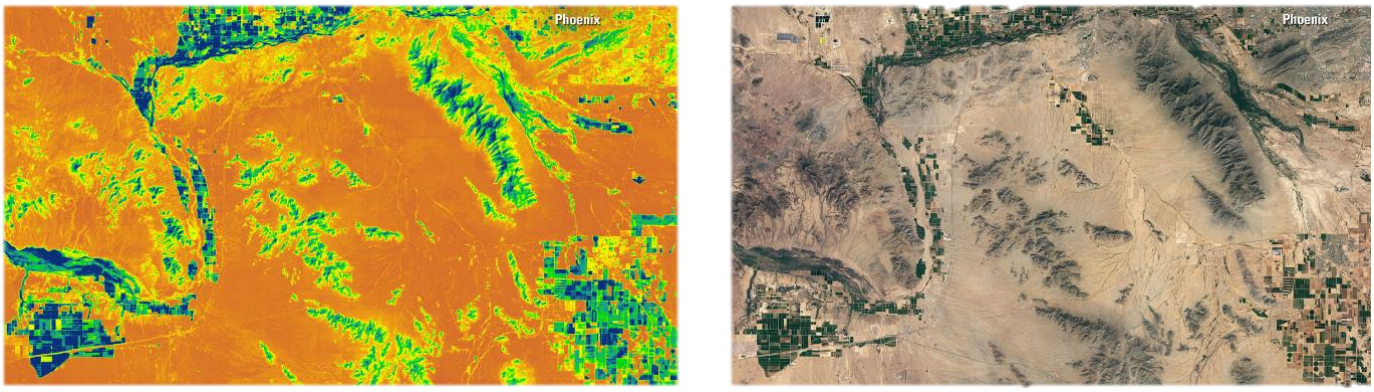

Figure 5 Evapotranspiration Map of the Colorado River Basin [10]

Close-Range Sensors

While satellites like those used in the Landsat Missions have gathered extremely valuable data over the past decades, the use of satellite imagery is not always perfect for the study of vegetative health. Satellite-based NDVI observation of plant heath has the potential to be influenced by certain non-vegetative variables. These include factors like moisture in the atmosphere, satellite geometry and calibration, as well as soil background and crop canopies [12]. Consequently, for some applications, using a close-range sensor is preferable over the use of satellites to perform NDVI analysis. Oklahoma State University addressed these concerns through the development of one such close-range sensor, the GreenSeeker™. The GreenSeeker™, like similar handheld NDVI sensors, compensates for atmospheric influence in readings by minimizing the effect of external light. The GreenSeeker™ accomplishes this by maintaining close range during data collection, as well as introducing its own light source. This offers a dual purpose: to decrease the influence of sunlight and to allow readings to be taken at any time of the day or night [12]. Handheld sensors such as this one also offer an additional advantage of increased resolution. While satellites offer the ability to scan extremely large areas of land, the resolution is not precise enough to study a single plot. The GreenSeeker™ offers high resolution and a high sample rate of approximately one-thousand measurements per second [12]. This allows an agriculturalist to easily and efficiently measure the infrared reflectivity of their crop for NDVI analysis. Researchers at the International Maize and Wheat Improvement Center (CIMMYT) were able to demonstrate the impact of handheld sensors like the GreenSeeker™. They utilized NDVI readings from the sensor to study proper allocation of land resources for the growth of maize and wheat in El Batán in the semiarid, subtropical highlands of central Mexico. The ability to gather accurate NDVI readings of relatively small plots was integral in their analysis of crop growth [12].

Another common use of close-range NDVI sensors is in the management of turf grass. Again, because of the relatively small land area being studied, close-range sensors become necessary for this application. One such sensor is the FieldScout TCM 500 NDVI Turf Color Meter. This sensor was developed to replace the visual evaluation of turf grass. Commonly, turf grass is evaluated by eye on a scale of one, representing dead grass, to nine, representing the most-healthy grass [13]. As discussed previously, however, visual evaluation is often subjective and inevitably varies based on individual biases. Accordingly, the FieldScout can be used to normalize the evaluation of turf grass. The FieldScout measures a three-inch diameter section of turf grass using an internal light source. It picks up light in the red (660 nm) and near infrared (850 nm) bands to report NDVI as a fraction, a percent reflectance, or a grass index from one to nine [13].

While handheld sensors such as these offer advantages, one of the main problems with their widespread utilization is the cost. The GreenSeeker™ costs $495 and the FieldScout costs $899 from their respective manufacturers. While the fields of agriculture and turf grass management could benefit greatly from the introduction of normalized analysis of plant health, the cost of using these close-range sensors is simply not feasible for many applications. This again suggests the potential impact of the research presented here: the utilization of inexpensive UAVs for NDVI analysis. This could provide the average agriculturalist the opportunity to take advantage of potentially industry-changing technology.

Aerial Sensors

Another alternative to satellite sensors is the use of aerial sensors. Airborne cameras capable of capturing multiple bands of the light spectrum can be used on manned aircraft to capture images of multiple plots of land. Like gathering images with satellites, using aerial sensors offers agriculturalists the ability to study large plots of land but gives a resolution closer to that of handheld sensors. This offers the convenience of studying entire crops at once but with an accuracy high enough to be useful for individual farmers to gather vital information. Terravion is one company that provides aerial image capturing for agricultural analysis. Terravion offers its customers weekly fly-overs during the growing season, delivering aerial images in color, NIR, NDVI, and thermal [14]. Farmers can identify all areas of plant growth, which show up as bright red in a NIR image, areas of high temperature or low moisture with the thermal image, and areas of unhealthy plant growth with the NDVI image. One such NDVI image captured by aerial analysis is shown in Figure 6 [14]. Here, the NDVI image gathered is post processed to develop a color map showing healthy areas in orange and red while displaying unhealthy areas in blue.

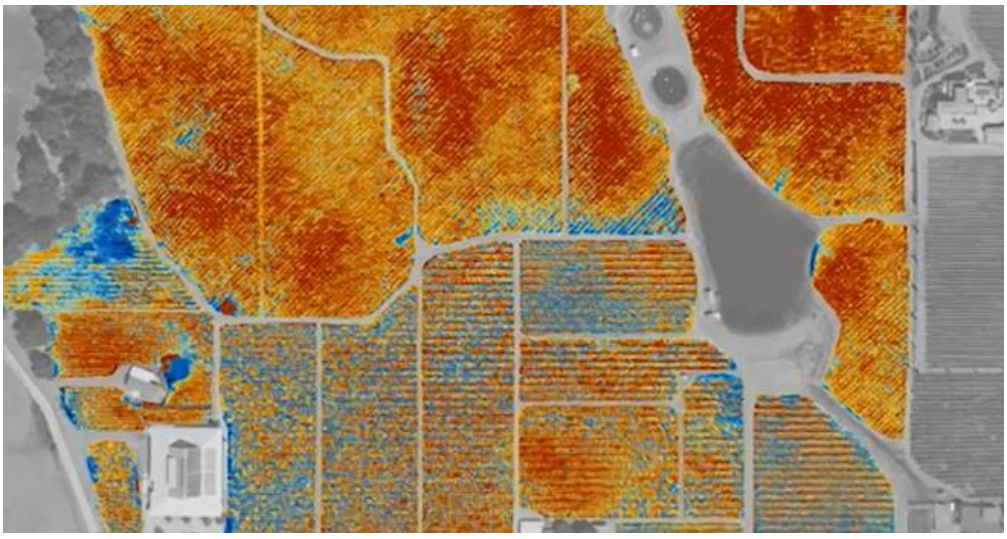

Figure 6 NDVI Image of Farmland Captured with Aerial Camera on Manned Aircraft [14]

The images Terravion provides capture data with a resolution of eighteen centimeters [14]. While this is far from the resolution of handheld sensors, it is significantly better than satellite images and typically sufficient for standard crops. Although aerial imaging using manned flights is promising for NDVI analysis of agricultural health, there are many overhead costs, which still make widespread use difficult. Terravion's image capturing service not only requires a camera capable of picking up the appropriate bands of light, it is also dependent on a plane and a pilot.

Instead of using manned flights, recent developments have reduced the size and weight of the cameras used to measure NDVI to allow for use on UAVs. The Tetracam ADC Micro, for example, measures only 6.55 mm x 4.92 mm and weighs 90 grams. It can record green, red, and NIR offering the necessary bands for NDVI calculations in images with 2048x1536 pixels. The resolution of the images captured is a function of altitude as detailed in Table 3 below [15].

Table 3 Tetracam ADC Micro Image Resolution [15]

Altitude Above Ground	Ground Resolution
122 m (~400 ft.)	4.63 cm
213.4 m (~700 ft.)	8.1 cm
365.8 m (~1200 ft.)	13.9 cm
915 m (~3000 ft.)	34.7 cm

Cameras like the Tetracam ADC Micro make utilizing UAVs for NDVI analysis possible but yet again, the cost of $4,000 is the limiting factor [15]. In order to make UAV-based NDVI analysis a feasible solution, a more cost-effective solution must be implemented. This research

looks to adapt standard cameras for use in NDVI analysis to replace the expensive NDVI cameras currently used to create an affordable platform for everyday agriculturalists.

Chapter 3 Utilizing Standard Cameras in NDVI Analysis

The main issues facing agriculturalists looking to use NDVI analysis for the study of plant health is the cost and resolution of the current platforms available for capturing NDVI images. Satellite images provide a view of large areas of land over long periods of time, but are not effective for studying individual plots of land. Close range sensors and aerial sensors on manned aircraft offer the ability to capture NDVI images with sufficient resolution but are far too expensive to be practical for most applications. One potential alternative that would make NDVI image capture more affordable is to find a way to use standard digital cameras. This can be done using filters.

When a digital camera records an image, it stores photons in millions of small cavities known as photosites. When exposure begins in order to capture an image, each of these is activated to gather photons. In order to distinguish between the different spectral bands, filters are placed over the photosites such that only red, green, or blue light can enter and be captured. Photosites are organized into a matrix known as a Bayer Array as shown in Figure 7 [16].

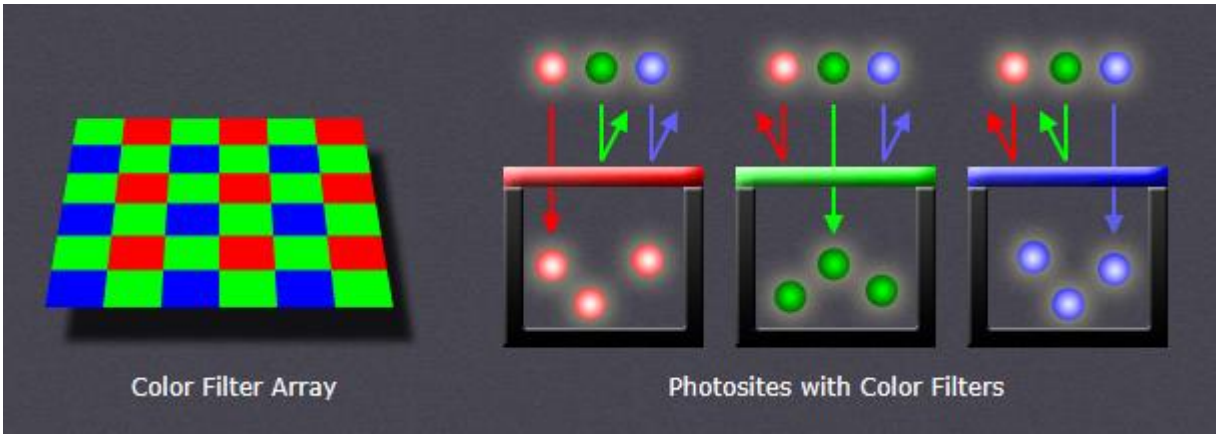

Figure 7 Bayer Array Organization [16]

Notice that in a Bayer Array, there are twice as many green photosites as red or blue. This is because the human eye is more sensitive to green light. By having an uneven distribution of photosites, the image that is captured appears less noisy and has a greater level of detail [16]. This filter mosaic typically does not block NIR light. In order to match the human eye, which cannot see NIR light, an internal NIR blocking filter is used in front of the entire array or is built into the lens coating. Typically, more expensive cameras that capture higher-quality images contain this kind of NIR filter. In order to perform NDVI analysis, however, the camera being used would need to have the ability to capture NIR light. While it could be feasible to remove the NIR blocking filter from high-quality cameras, less expensive cameras typically do not contain NIR filters. Thus, by using less expensive cameras, NIR light could be captured and thus could be used to mimic NDVI analysis.

While cameras without an NIR filter have the potential to be used for NDVI, a method must be used to distinguish between NIR light and RGB light captured in photosites. This can be accomplished with filters. For example, Figure 8 below shows transmittance as a function of wavelength for light passing through blue filters [17, 18]. The blue filters allow blue light to pass through but block green and red light. Consequently, light entering the green and red photosites has been filtered to block all three RGB wavelengths of light, leaving only NIR wavelengths. The blue photosites collect both blue and NIR light. As such, by modifying Equation 1 to account for NIR light on the red and green channels while using the blue channel as the red equivalent, NDVI can be calculated. This is shown in Equation 2.

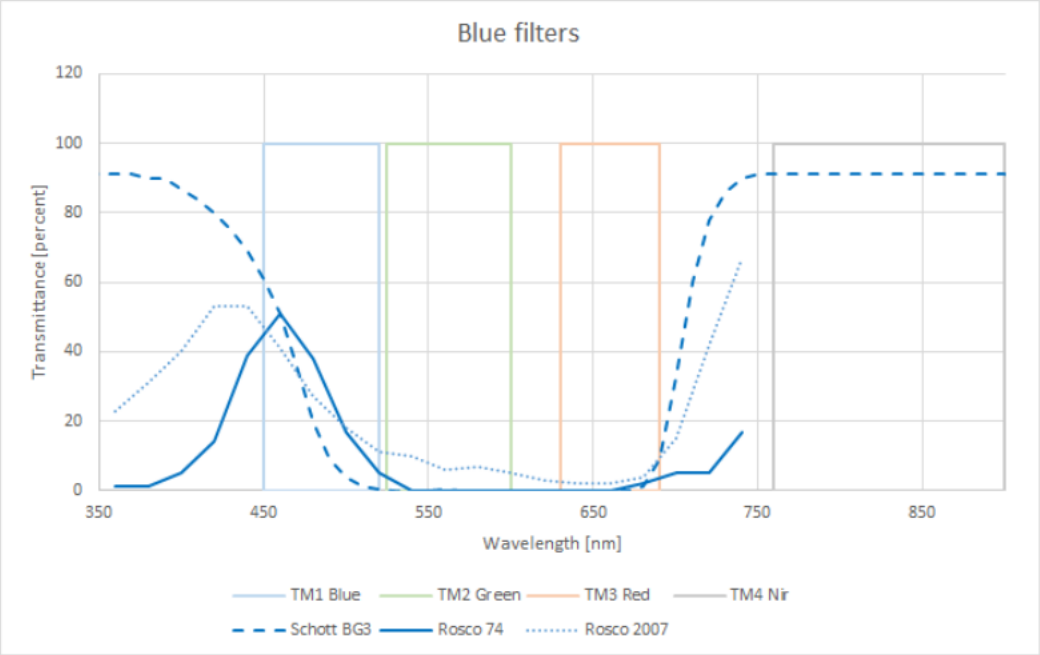

Figure 8 Wavelength Transmittance using Blue Filters [17, 18]

$$\text{NDVI} \approx \frac{(\text{red} + \text{green}) - \text{blue}}{(\text{red} + \text{green}) + \text{blue}} \qquad \text{[Eq. 2]}$$

This concept can be repeated with other types of filters. For instance, a red filter would allow red light to pass but would block blue and green light. Thus, NIR light would be captured by the blue and green photosites while red light plus NIR would be captured in the red photosites. This is shown in Figure 9 [17, 19]. By again modifying Equation 1, NDVI could be measured through Equation 3.

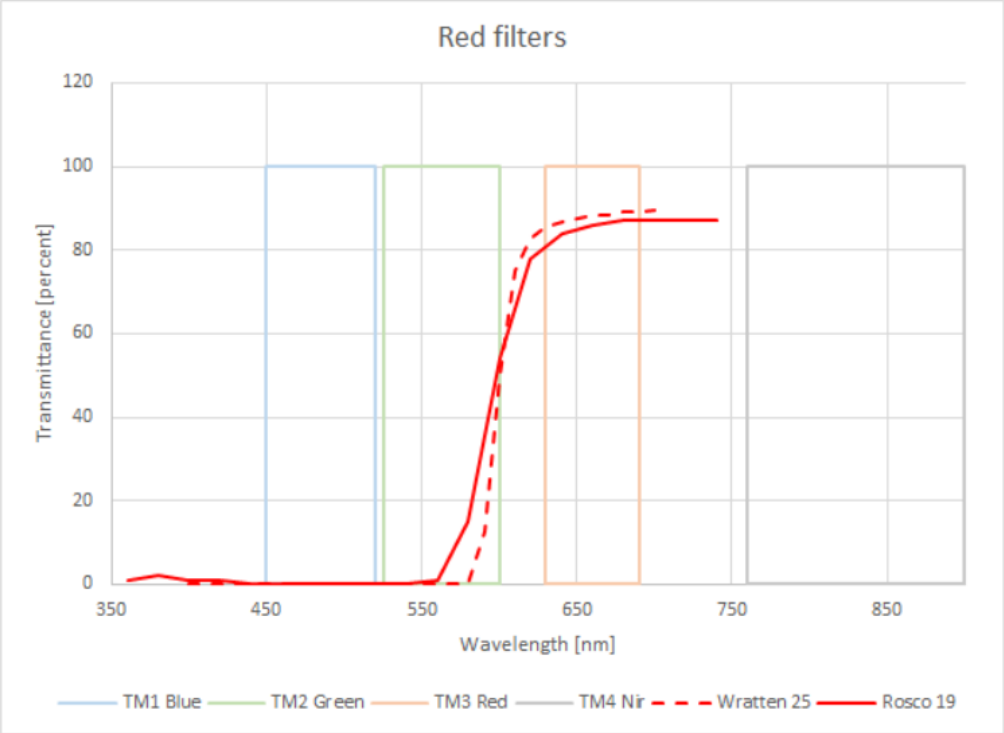

Figure 9 Wavelength Transmittance using Red Filter [17, 19]

$$\text{NDVI} \approx \frac{(\text{blue} + \text{green}) - \text{red}}{(\text{blue} + \text{green}) + \text{red}} \qquad \text{[Eq. 3]}$$

Finally, an orange filter can be used to block blue light as demonstrated in Figure 10 [17, 19]. In this case, the blue channel would capture only NIR light while the red and green channels would capture their respective colors as well as NIR light. Equation 4 could accordingly be used to compare the NIR light in the blue and red channels. Alternatively, the green channel could be used in a similar way.

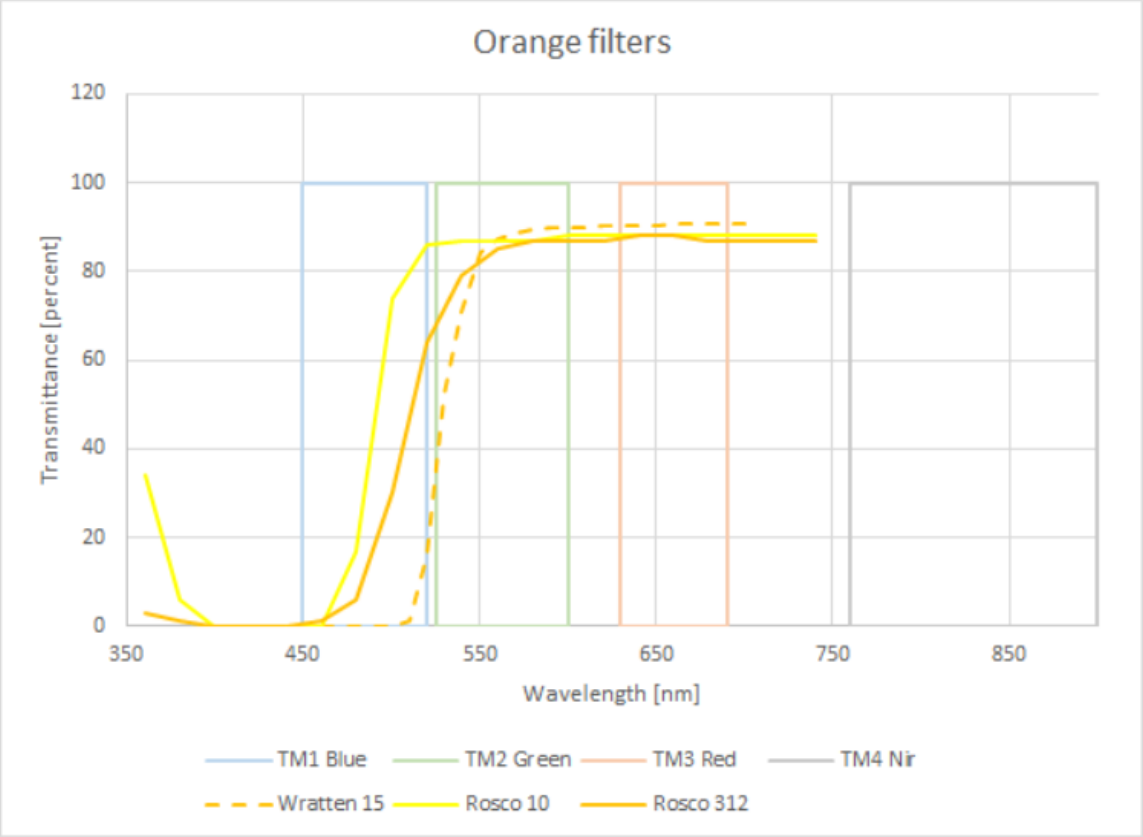

Figure 10 Wavelength Transmittance using Orange Filter [17, 19]

$$\mathrm{NDVI} \approx \frac{\mathrm{blue} - \mathrm{red}}{\mathrm{blue} + \mathrm{red}} \qquad \text{[Eq. 4]}$$

Chapter 4 Hardware Development

In order to implement an unmanned aerial system for NDVI analysis of agricultural health, the first element that needed to be considered was the hardware that would be utilized. Selection of an appropriate UAV platform proved to be a crucial process for the success of this research. The primary focus was to construct a system that could marketed for use by agriculturalists. In order to be attractive to farmers with little experience in flying unmanned aircraft or with image processing, the platform would have to be easy to learn, intuitive to use, and have a simple system for post-processing images. Additionally, one of the primary focuses of this research is to make NDVI analysis more practical for widespread use. As such, one of the primary users that needs to be considered is small-scale farmers without the capital to pay for more expensive options for NDVI analysis such as the services offered by Terravion. Keeping the platform inexpensive was therefore of large concern. The types of cameras that could be used also had to be considered. Many of the UAVs on the market today come with mounted cameras. In order to perform a modified NDVI analysis using the filter techniques discussed in Chapter 3, a UAV equipped with a mounted camera that did not have a NIR filter would be necessary, unless modification to remove the filter could be performed. Alternatively, we considered UAVs with the ability to attach or remove hardware. In this case, we could select a UAV and an appropriate camera to combine into a finalized platform. The following chapter details the various hardware considered for an NDVI analysis platform

Training Platforms

The first consideration both for internal research purposes and for use by agriculturalists was selection of training platforms. There are a wide array of small, inexpensive UAVs available to hobbyists. These platforms typically do not fly as well in high wind or altitudes as larger platforms and have much lower quality images but have important qualities for training purposes: they are inexpensive and durable. As such, investigation into UAVs began with small training vehicles to help users learn techniques before flying more expensive platforms. Three UAVs were utilized for this research.

The first was the Hubsan X4 (H107C HD) 4 Channel 2.4GHz RC Quadcopter pictured in Figure 11 [20]. Of the UAVs investigated, this one was the least expensive and easiest to fly. It has a 720p HD camera that records video directly to a memory card onboard the platform. The data sheet for this UAV in Table 4 details its specifications. It served as an ideal training vehicle because of its extremely stable flight and inexpensive replacement parts in the event of a crash. Its downside, however, is that it did not offer live first-person video (FPV). In order to fly over a larger field of crops, a pilot would need to be able to fly out of the direct line of sight and utilize an on-board camera to track flight. In order to train for this type of flight, a UAV with FPV capability would be necessary.

Figure 11 Hubsan X4 H107C HD [20]

Table 4 Hubsan X4 H107C HD Specifications [20]

Price	$80
Size	2.7 x 2.7 x
Weight	1 lb. 2.4 oz.
Resolution	1280 x 720
RGB Capture	Yes
NIR Capture	No
Internal NIR Filter	No
Flight Time	7 min
Charging Time	40 min

Conveniently, Hubsan also produces a slightly more expensive version of the X4 model that utilizes FPV, the Hubsan X4 H107D FPV RC Quadcopter with Live LCD Transmitter. This UAV is a similarly sized vehicle that transmits live video to a display on the controller seen in Figure 12 [21]. It allows users to train how to fly out of the direct line of sight using the onboard

camera. This mimics the flying conditions of large-scale UAVs more effectively and allows users to become more comfortable piloting a vehicle using only a display rather than relying on visual cues. One downside, however, is that image quality is lower because rather than recording video directly on the vehicle, it is streamed live to the controller. The rest of the specifications for the X4 H107D FPV are shown in Table 5 [21]. Regardless of the low image quality, this UAV provides a realistic platform for training new pilots.

Figure 12 Hubsan X4 H107D FPV RC Quadcopter with Live LCD Transmitter [21]

Table 5 Hubsan X4 H107D FPV Specifications [21]

Price	$200
Size	4.75 x 4.75 x
Weight	1 lb. 2.4 oz.
Resolution	640 x 480
RGB Capture	Yes
NIR Capture	No
Internal NIR Filter	No
Flight Time	7 min
Charging Time	30 min

The last training platform used in this research was the Parrot AR Drone 2.0. This UAV, shown in Figure 13 is larger than the Hubsan vehicles and offers a flight experience more similar to that of high-performance vehicles while still maintaining the desired qualities of a training platform: easy and intuitive flight controls, and durability in the event of a crash [22]. It is controlled with an iPad application and is equipped with two cameras. The first is a high definition 720p forward-facing camera and the second camera pointed directly downward. Both record video during flight as well as stream video to the iPad application for FPV capability. Downward facing sensors measure and display altitude to the user during flight. It also has autopilot features such as a "Return Home" mode in which it will fly to a preset home location and land automatically. All these qualities allow a user to train on a vehicle similar in the size and performance to that of the more expensive platforms without worrying about easily damaged equipment. The specifications for this UAV are detailed in Table 6 [22].

Figure 13 Parrot AR Drone 2.0 [22]

Table 6 Parrot AR Drone 2.0 Specifications [22]

Price	$570
Size	23 x 23 x 5 in
Weight	0.93 lbs.
Resolution	1280 x 720
RGB Capture	Yes
NIR Capture	No
Internal NIR Filter	No
Flight Time	15 min
Charging Time	45 min

Application Platform

While the training platforms offered the ability to develop flight skills, a platform with a higher level of functionality and control was necessary for experimental data collection. Nevertheless, cost and ease-of-use were important factors to keep the feasibility of implementing this system as a tool for agriculturalists. For these reasons, the Phantom 2 Vision + shown in Figure 14 was chosen for the purposes of this research [23]. The Phantom 2 Vision +, referred to for the remainder of this paper as "the Phantom," is equipped with a high performance camera which shoots full HD video at 1080p/30fps and 720p/60fps offering both real-time and slow-motion image capture at 14 megapixels. The camera is mounted on a gimbal, which stabilizes the camera and allows the user to change the tilt angle of the camera during flight. It records images on a 4GB micro SD onboard as well as streams live FPV perspective to the user through a compatible smartphone application. The Phantom also has highly precise flight controls. The integrated GPS

system offers autopilot capabilities including position and altitude lock, stable hovering, and return-to-home modes. Its ground station support utilizes GPS to allow for flight planning with up to sixteen waypoints. The Phantom's specifications are shown in Table 7 [23].

Figure 14 Phantom 2 Vision + [23]

Table 7 Phantom 2 Vision + Specifications [23]

Price	$1369
Size	17 x 8.1 x 12.5 in
Weight	2.72 lb.
Resolution	4384 x 3288
RGB Capture	Yes
NIR Capture	No
Internal NIR Filter	No
Flight Time	20 min
Charging Time	45 min

Data Collection

Using the Phantom, data was able to be collected to test the feasibility of using a UAV to study agricultural health. Images were collected at the Russel E. Larson Agricultural Research Center located southwest of Penn State University as shown in the map in Figure 15. Several different crops are grown in plots at the Research Center. For the purposes of this research, aerial pictures were taken of the apple orchard plots.

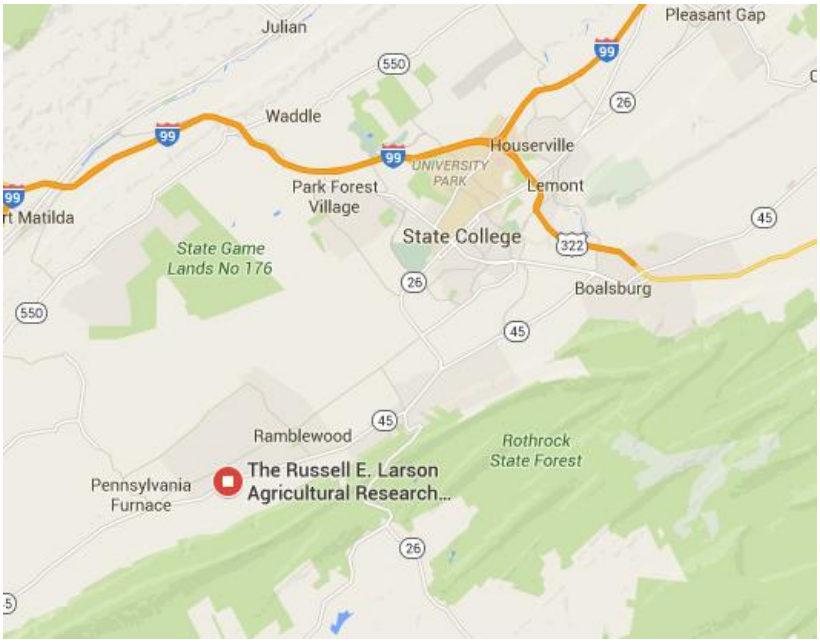

Figure 15 Data Collection Site [24]

The purpose of collecting data at this time was twofold: to evaluate the feasibility of using a UAV to take aerial pictures of a crop and to test the path planning capabilities which could expedite the evaluation of health using NDVI analysis. In this process, the first step was to document the plots of interest with aerial pictures taken with the Phantom. Figure 16 shows a satellite image of the apple orchard plots at the Research Center. Photos were taken with the

Phantom of plots A1 through A3 as well as plot C. Figure 17 through Figure 19 show aerial photos of the A-block plots taken with the Phantom's onboard camera. These images were captured at an altitude of 250 feet and have been post-processed to remove barrel distortion. The rows are labeled with a one or two lettered identification and yellow boxes mark rows for which the Phantom took pictures. Figure 20 is a satellite image of Plot C. Potential flying hazards were also identified such as a power line in Figure 17 marked with a red line. These images were captured in April of 2015, before the blossom season for apples.

Figure 16 Satellite Image of Apple Orchard Plots

Figure 17 Undistorted Image of Plot A1 at 250 feet

Figure 18 Undistorted Image of Plot A2 at 250 feet

Figure 19 Undistorted Plot of A3 at 250 feet

Figure 20 Satellite Image of Plot C

Current methods for NDVI analysis such as image capture using satellites or manned aircraft offer helpful data but are limited to an aerial perspective looking directly downward on a plot from above. For a crop such as apple trees, which contain fruit throughout a large volume of branches and leaves, this perspective may not give the best information. One of the advantages of capturing data with UAVs is the ability to manipulate altitude and camera angle to view multiple perspectives of a crop. In order to test the advantage of this system, a comparison was made between direct overhead images and images taken at a 45-degree camera angle. Figure 21 shows an image of three rows of trees at an altitude of 50 feet taken from directly above. Figure 22 shows an image of the same three rows taken at a 45-degree angle from the side. It is clear that a larger portion of the tree can be seen in the second image, clearly demonstrating an advantage in using UAVs to study this kind of agriculture. Figure 23 shows another set of three rows just before the apple crop harvest. Here it can again be seen that image capture at an angle provides a clear view of the entire apple growth on the trees. These images were taken directly from the Phantom before any post-processing and a large degree of barrel distortion can be seen. Steps to remove this distortion will detailed in Chapter 5.

Figure 21 Image of Three Rows at 50 feet Overhead

Figure 22 Image of Three Rows at 50 feet (45 Degree Angle)

Figure 23 Image of Apple Crop Before Harvest (45-Degree Angle)

By capturing images at a lower altitude and from an angle rather than from directly above, a UAV offers the ability to gather more useful data for NDVI analysis. However, because images are captured a closer distance, more images need to be taken to collect data for an entire crop. Luckily, one aspect of the Phantom's compatible application is flight planning. This application can be downloaded to a smartphone or tablet and connects with the GPS system on the Phantom. For flight planning, it provides a satellite image of the Phantom's current location and allows the user to define up to sixteen waypoints to create a flight path for the Phantom. The user can set the location of waypoints and specify the desired altitude at each. The Phantom will then fly to each location and return to home. During flight, the user can manipulate the camera angle and direction, maintaining full control of image capture. As such, a farmer wishing to utilize the Phantom for NDVI analysis could simply define a path around their crop, capturing useful data quickly and easily. Using this method along with manual flight, images and video were taken of all of the rows of apple trees defined in Figure 17-Figure 23.

Chapter 5 Software Development

In order to provide full NDVI analysis of a crop using the Phantom, several post-processing techniques need to be utilized. First, barrel distortion needs to be removed from the images, such as that seen in Figure 21-Figure 23. Additionally, in order to view an entire area of a crop, individual images need to be stitched together using a post-processing algorithm. Lastly, to obtain an evaluation of plant health, filters discussed in Chapter 3 along with a post-processing technique must be utilized to obtain a pseudo-NDVI images that provide the same health information without requiring an expensive NDVI camera. The following sections will detail each of these processes. For the purposes of this research, MATLAB was utilized for software implementation.

Barrel Distortion Removal

There are two main types of distortion that can affect an image: perspective and optical. Perspective distortion occurs when the dimensions of an object photographed seem skewed due to the angle of the camera when the image was taken [25]. This type of distortion is unlikely to have an effect on images captured for agricultural analysis, but optical distortion is of greater concern. There are three types of optical distortion, also known as radial distortion. These include barrel, pincushion, and mustache, each named due to the shape of the distortion. Barrel distortion is of most importance to this research because it is an effect commonly seen in images taken with a wide-angle lens, such as the lens in the camera on the Phantom. The field of view in a wide-angle lens is larger than the size of the image sensor that captures the images. As such, the image needs to be squeezed to fit into the frame. When this occurs, the image appears to bend, particularly near

the edges. Figure 24 shows an undistorted grid in comparison with a grid exhibiting strong barrel distortion [24].

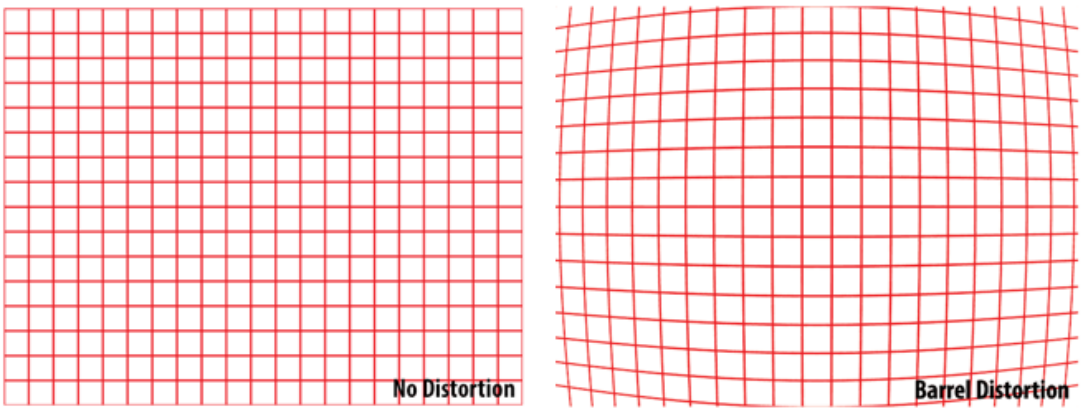

Figure 24 Distortion Comparison [25]

In order to adjust for this effect, geometric camera calibration can be performed. Camera calibration estimates the parameters of a lens, which can then be used for a number of purposes including measuring the size of an object, determining the location of an object in a scene, or to correct for lens distortion such as barrel distortion as shown above. The camera parameters that need to be solved for include intrinsics, extrinsics, and distortion coefficients. Extrinsic parameters include rotation and translation while intrinsic parameters consist of the focal length, optical center, and the skew coefficient. Lastly, the distortion coefficients represent the radial distortion of the lens. To solve for the intrinsic and extrinsic parameters, multiple images need to be taken to determine correspondences between 3D world points and 2D image points. This is typically done with a checkerboard pattern as shown in Figure 25 [27]. These correspondences can then be used to solve for intrinsic and extrinsic parameters, which make up the camera matrix. The camera matrix defines the characteristics of the camera and maps the 3D world into the 2D image plane.

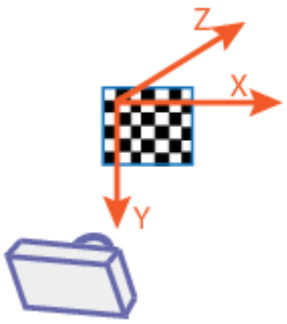

Figure 25 Camera Calibration Card [25]

While the camera matrix defines many physical properties, it is based on a model of a pinhole camera, which does not include a lens. Consequently, distortion parameters must be determined to model lens properties. Barrel distortion is a type of radial distortion and is therefore modeled by radial distortion coefficients. Equations 5 and 6 show how the pixel locations in a distorted image ($x_{undistorted}$, $y_{umdistorted}$) are mapped to the pixel locations in an undistorted image (x, y) using the radial distortion coefficients (k_1, k_2, and k_3). The variable r^2 in this equation is equivalent to x^2+y^2. It should be noted that x and y are in normalized image coordinates which are calculated by translating to the optical center and dividing by the focal length in pixels and thus, x and y are dimensionless [26].

$$x_{distorted} = x(1 + k_1 * r^2 + k_2 * r^4 + k_3 * r^6) \quad \text{[Eq. 5]}$$

$$y_{distorted} = y(1 + k_1 * r^2 + k_2 * r^4 + k_3 * r^6) \quad \text{[Eq. 6]}$$

The barrel distortion in an image can accordingly be removed by calibrating the radial distortion coefficients. Figure 26 shows an image of three rows of apple trees taken by the Phantom before barrel distortion was removed. Figure 27 shows one of the undistorted overhead images from Chapter 4 where the effect of the distortion removal is evident in the straightness of the rows.

Figure 26 Phantom Image with Strong Barrel Distortion

Figure 27 Phantom Image with Barrel Distortion Removed

Image Stitching

The intent of this research is to develop a system that would allow agriculturalists to analyze the health of a crop more easily. The desired result would be to supply a pseudo-NDVI

image of an entire plot in order to give a clear overview of areas that are unhealthy. Doing so would require compiling several images of small sections together to form one image. This can be performed using a method called image stitching. Image stitching algorithms are commonly used to form panoramic images. MathWorks® offers information on how to perform this type of process on a set of images in MATLAB using feature based image registration techniques. To form a panoramic image, an iterative set of commands are used to detect common features in adjacent images and blend a pre-defined set of images into a one single panorama. The code to perform this process is included in Appendix A [26]. This code first loads the set of images and arranges them in a 2-D array. For example, Figure 28 shows a set of images provided by MathWorks® of their headquarters in Boston, Massachusetts [27]. These images were taken on a smart phone with an uncalibrated camera. The five images were captured sweeping left to right across the building. The algorithm then matches features iteratively between each image I(*n*) and the image preceding it I(*n-1*). It then estimates and computes the geometric transformation between I(*n*) and I(*n-1*). Next, the algorithm finds the x-limits of the transforms and determines the image closest to the center, assuming that the scene is horizontal. Lastly, it maps and overlays the images over each other to create a full panorama. The final result is shown in Figure 29 [27].

Figure 28 Image Array [27]

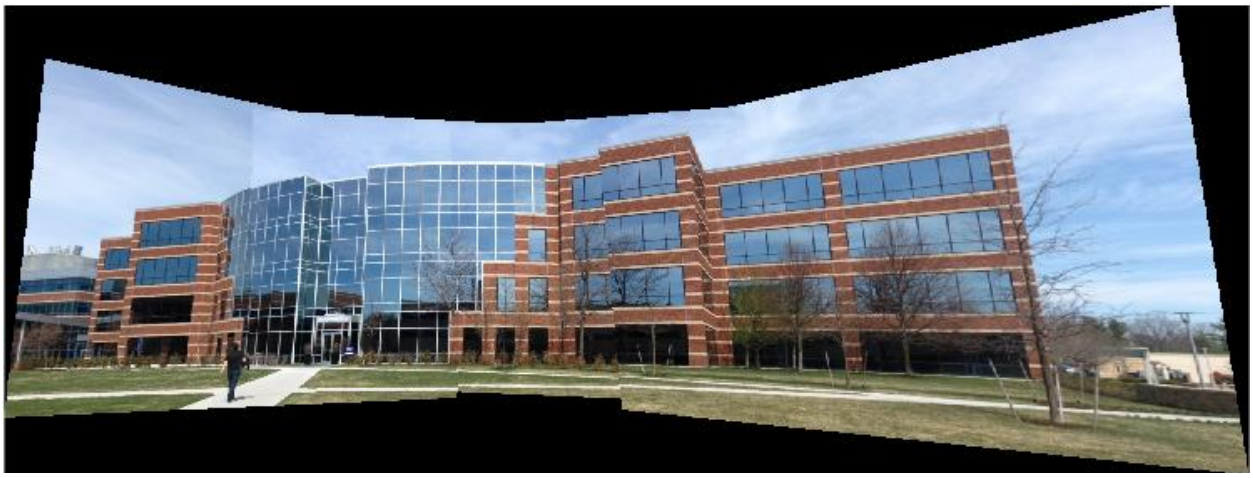

Figure 29 Panorama Image [27]

Pseudo-NDVI

The final post-processing step that must be taken in order for the images captured with a standard non-NDVI camera to function as a method for the evaluation of plant health is to utilize the filter methods discussed in Chapter 3 to produce an equivalent, or pseudo-NDVI, scale. As previously mentioned, when a filter is placed over a camera without a NIR-blocking filter, standard RGB channels can be used to evaluate NDVI using an adjusted equation. This process was tested using an image of turf grass. The original image, shown in Figure 30, was taken using a camera without a filter. The same area of grass was then captured using a red filter, shown in Figure 31. In this second image, NIR light was captured on the blue channel while red light plus NIR was captured on the red channel. Using Equation 3, it was possible to produce an image that depicted healthy areas in green while showing unhealthy areas in red. This result can be seen in Figure 32. It can be noted that the areas of dead grass in Figure 30 appear as red in Figure 32, thus confirming the effectiveness of the evaluation. This conversion was completed with a MATLAB script developed by Dr. Sommer, which is detailed in Appendix B.

Figure 30 Grass Plot Captured with Unfiltered Camera

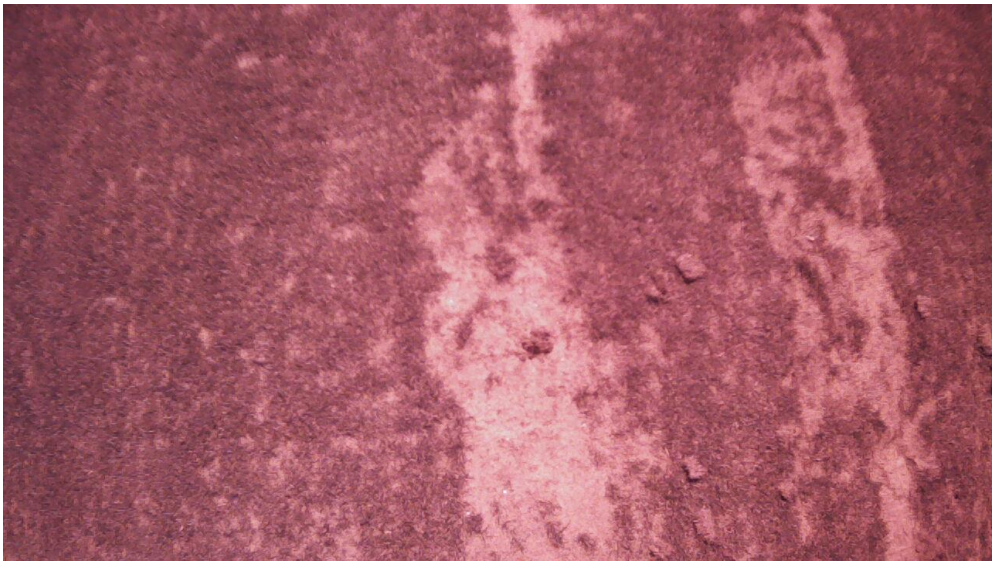

Figure 31 Grass Plot Captured with Red Filter

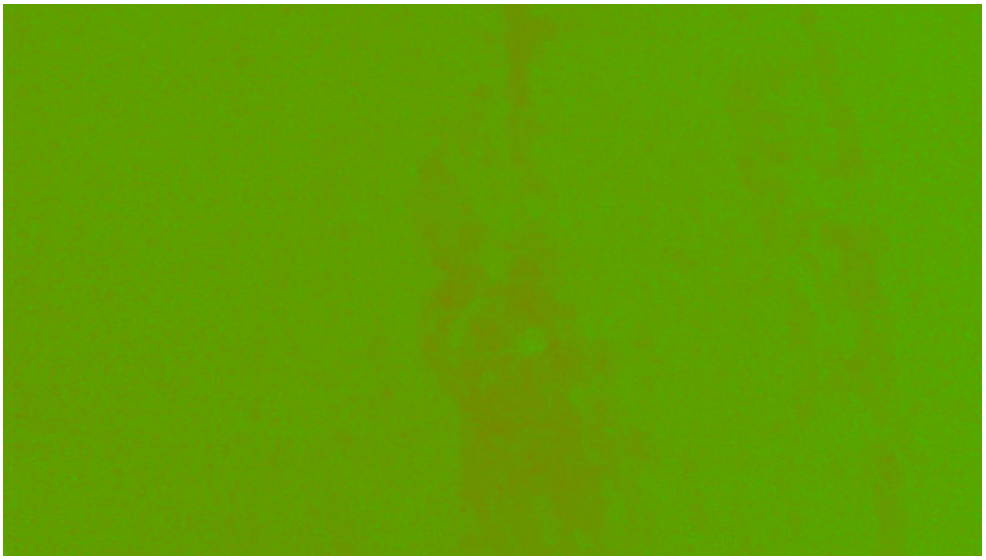

Figure 32 Pseudo-NDVI Image of Grass Plot

Chapter 6 Conclusion

The purpose of this research effort was to explore the feasibility of utilizing UAVs as an inexpensive alternative to the procedures currently used for NDVI analysis, thus allowing this technology to be more widely available to agriculturalists. In order to be feasible as a small-scale platform for NDVI analysis, a UAV-based system would need to be able to provide equally useful information as that of standard NDVI analysis systems such as satellites or manned aircraft but also be less expensive and easily implemented by those who would benefit from its use. Several different platforms were explored and it was clear that a combination of training platforms along with the Phantom 2 Vision + could allow novice pilots to become skilled enough to capture their own images for analysis. Specifically, the Phantom was shown to be an example of how a relatively inexpensive UAV could utilize path-planning software to quickly and effectively capture images of an area of crop. These images could not only match the type of overhead images used for NDVI analysis, but also in some applications exceed the quality of data collected by utilizing camera angles which offer more information, such as the volume of apples yielded in a row of trees.

One of the major keys to replacing expensive NDVI camera equipment is the use of inexpensive cameras to provide pseudo-NDVI images. Filter technology was explored which would make this process possible. It was shown that MATLAB could be used to take images from a standard camera, remove any distortion in the image, stitch multiple images together, and convert an image into a color map showing healthy and unhealthy areas using a modified NDVI equation. All these factors culminate in the conclusion that

it is feasible to implement a UAV platform to perform NDVI analysis, thus bypassing the need for expensive equipment or professional personnel to offer scientific data on the health of a crop. By making NDVI analysis inexpensive and easy to implement, it is possible to implement this technology on a widespread basis, altering the way agriculturalists manage plant health and utilizing modern technological advances to revolutionize the agricultural industry as a whole.

Future Work

While progress has been made in implementing a UAV-based system for NDVI analysis, there is still work to be done. It has been shown that a camera mounted on a UAV can be used to capture images for NDVI analysis. However, it is unclear how ambient light may affect this process. Taking images at different times of day or in different weather may affect the consistency of results. Study is necessary to determine the magnitude of this potential effect and how to mitigate complications if necessary. One possible technology worth investigating is the Sequoia sensor by MicaSense. The Sequoia, shown in Figure 33 below, consists of two sensors mounted on the top and bottom of a UAV which capture both ambient light from above and light reflected from surfaces below. Using this information, it is possible to normalize data to remove the effect of ambient light.

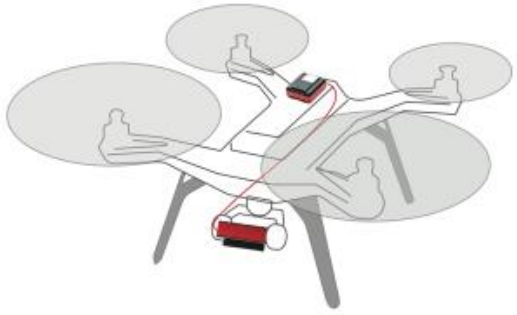

Figure 33 Sequoia Sensor [28]

Additionally, it is worth investigating other software to perform post-processing techniques such as image stitching. One such software package is Pix4D. This software allows a user to perform path-planning operations through a smartphone application. The user can define a rectangular area for the UAV to fly over and the Pix4D software defines a flight path, collects a set of images during flight, and provides a stitched image of the entire area after the flight [28].

This was tested during research, but changes in the Phantom's automatic white balance caused issues during the image stitching process. The problem arose from the fact that in order to operate the Pix4D application, the user needed to exit the application used to operate the Phantom, thus removing the ability to adjust white balance settings. As a result, the Phantom utilized the default auto white balance setting, which caused inconsistences in the individual images collected. However, given the potential impact of the Pix4D software, it is worth investigating if utilizing a different UAV could solve this issue.

Lastly, the software code used in the research was developed using MATLAB. While this was able to demonstrate the feasibility of post processing the images from a UAV-based system to provide NDVI analysis, it is the ultimate goal to make this platform as inexpensive as possible. As such, it is desirable to develop code that does not require a MATLAB license to operate. Future work should focus on utilizing a more-universal coding language like C to develop similar code that could be more widely implemented.

BIBLIOGRAPHY

[1] Reagan, Jason, 2015, “How Low Will Drone Prices Go?” from http://dronelife.com/2015/07/09/how-low-will-drone-prices-go/

[2] Pogue, David, 2016, “Exclusive: Amazon Reveals Details About Its Crazy Drone Delivery Program.” from https://www.yahoo.com/tech/exclusive-amazon-reveals-details-about-1343951725436982.html

[3] Pettit, Jeniece, 2015, “How Drones are Being Used for Safety and Rescue.” from http://www.cnbc.com/2015/11/20/how-drones-are-being-used-for-safety-and-rescue.html

[4] Honsberg, Christiana and Bowden, S.,nd., “Energy of Photon.” from http://www.pveducation.org/pvcdrom/properties-of-sunlight/energy-of-photon

[5] Helioseptra, 2012, “Which Regions of the Electromagnetic Spectrum do Plants Use to Drive Photosynthesis?” from https://www.heliospectra.com/sites/default/files/general/What%20light%20do%20plants%20need_5.pdf

[6] Nave, R, n.d., “Light Absorption for Photosynthesis.” from http://hyperphysics.phy-astr.gsu.edu/hbase/biology/ligabs.html

[7] Agribotix, 2014, “Misconception about UAV-Collected NDVI Imagery and the Agribotix Experience in Ground Truthing these Images for Agriculture.” from misconceptions-about-uav-collected-ndvi-imagery-and-the-agribotix-experience-in-ground-truthing-these-images-for-agriculture

[8] “How to Practice Integrated Pest Management” from http://www.fao.org/agriculture/crops/thematic-sitemap/theme/spi/scpi-home/managing-ecosystems/integrated-pest-management/ipm-how/en/

[9] USGS, 2015, “Landsat Missions: Imaging Earth Since 1972.” from http://landsat.usgs.gov/about_mission_history.php

[10] NASA, n.d., “Landsat 1.” from http://landsat.gsfc.nasa.gov/?p=3172

[11] USGS, 2016, “Frequently Asked Questions about the Landsat Missions.” from http://landsat.usgs.gov/band_designations_landsat_satellites.php

[12] Verhulst, N., and Govaerts, B. , 2010, “ The Normalized Difference Vegetation Index (NDVI) Greenseeker™ Handheld Sennsor: Toward the Integrated Evaluation of Crop Management. Part A- Concepts and Case Studies,” CIMMYT Institutional Mulitmedia Publications,” pp. 1-4.

[13] Spectrum Technologies, Inc., n.d., “To Measure is to Know” from http://www.specmeters.com/nutrient-management/chlorophyll-meters/ndvi/tcm500/

[14] “Terravion.” from http://www.terravion.com/

[15] Tetracam Inc., 2015, “ADC Micro” from http://www.tetracam.com/Products-ADC_Micro.htm#Introduction

[16] Cambridge in Colour, 2016, “Digital Camera Sensors” from http://www.cambridgeincolour.com/tutorials/camera-sensors.h

[17] Rosco Laboratories, 2016, “How Color Filters Work” from http://www.rosco.com/filters/roscolux.cfm?menuReturn=filters

[18] Volume Precision Glass, Inc., n..d., “Schott_BG3_Filter” from http://www.vpglass.com/filter_glass/schott_bg3_filter_glass.html

[19] Peed, Allie C., n.d., “ Transmission of Wratten Filters” from http://www.karmalimbo.com/aro/pics/filters/transmision%20of%20wratten%20filters.pdf

[20] All-battery, 2016, “Hubsan X4 (H107C HD) 4 Channel 2.4GHz RC Quad Copter with 720p HD Camera” from http://www.all-battery.com/hubsanx4-h107chd-4channelrcquadcopterwithhdcamera-61170.aspx?variation=5349

[21] All-battery, 2016, “Hubsan X4 (H107D-FPV) RC Quadcopter Live LDC Transmitter” from https://www.all-battery.com/HubsanX4-H107D-FPVrcQuadcopterLiveLCDtransmitter-61150.aspx

[22] Parrot S.A., 2015, “A.R. Drone 2.0” from http://ardrone2.parrot.com/

[23] DJI, 2016, “Phantom 2 Vision + V3.0” from https://store.dji.com/product/phantom-2-vision-plus?position=1

[24] Google, “Google Maps” from https://www.google.com/maps

[25] Mansurov, Nasim, 2013, “What is Distortion” from https://photographylife.com/what-is-distortion

[26] Mathworks, 2016, “What is Camera Calibration” from http://www.mathworks.com/help/vision/ug/camera-calibration.html

[27] Mathworks, 2016, “Feature Based Panoramic Image Stitching” from http://www.mathworks.com/help/vision/examples/feature-based-panoramic-image-stitching.html

[28] MicaSense Inc., 2016, “Parrot Sequoia” from http://www.micasense.com/sequoia/

Appendix A

```
% Load images.
buildingDir = fullfile(toolboxdir('vision'), 'visiondata', 'building');
buildingScene = imageSet(buildingDir);

% Display images to be stitched
montage(buildingScene.ImageLocation)
```

```
% Read the first image from the image set.
I = read(buildingScene, 1);

% Initialize features for I(1)
grayImage = rgb2gray(I);
points = detectSURFFeatures(grayImage);
[features, points] = extractFeatures(grayImage, points);

% Initialize all the transforms to the identity matrix. Note that the
% projective transform is used here because the building images are fairly
% close to the camera. Had the scene been captured from a further distance,
% an affine transform would suffice.
tforms(buildingScene.Count) = projective2d(eye(3));

% Iterate over remaining image pairs
for n = 2:buildingScene.Count

    % Store points and features for I(n-1).
    pointsPrevious = points;
    featuresPrevious = features;

    % Read I(n).
    I = read(buildingScene, n);
```

```
    % Detect and extract SURF features for I(n).
    grayImage = rgb2gray(I);
    points = detectSURFFeatures(grayImage);
    [features, points] = extractFeatures(grayImage, points);

    % Find correspondences between I(n) and I(n-1).
    indexPairs = matchFeatures(features, featuresPrevious, 'Unique', true);

    matchedPoints = points(indexPairs(:,1), :);
    matchedPointsPrev = pointsPrevious(indexPairs(:,2), :);

    % Estimate the transformation between I(n) and I(n-1).
    tforms(n) = estimateGeometricTransform(matchedPoints, matchedPointsPrev,...
        'projective', 'Confidence', 99.9, 'MaxNumTrials', 2000);

    % Compute T(1) * ... * T(n-1) * T(n)
    tforms(n).T = tforms(n-1).T * tforms(n).T;
end
```

```
imageSize = size(I);  % all the images are the same size

% Compute the output limits  for each transform
for i = 1:numel(tforms)
    [xlim(i,:), ylim(i,:)] = outputLimits(tforms(i), [1 imageSize(2)], [1 imageSize(1)]);
end
```

```
avgXLim = mean(xlim, 2);

[~, idx] = sort(avgXLim);

centerIdx = floor((numel(tforms)+1)/2);

centerImageIdx = idx(centerIdx);
```

```
Tinv = invert(tforms(centerImageIdx));

for i = 1:numel(tforms)
    tforms(i).T = Tinv.T * tforms(i).T;
end
```

```
for i = 1:numel(tforms)
    [xlim(i,:), ylim(i,:)] = outputLimits(tforms(i), [1 imageSize(2)], [1 imageSize(1)]);
end

% Find the minimum and maximum output limits
xMin = min([1; xlim(:)]);
xMax = max([imageSize(2); xlim(:)]);

yMin = min([1; ylim(:)]);
yMax = max([imageSize(1); ylim(:)]);

% Width and height of panorama.
width  = round(xMax - xMin);
height = round(yMax - yMin);

% Initialize the "empty" panorama.
panorama = zeros([height width 3], 'like', I);
```

```
blender = vision.AlphaBlender('Operation', 'Binary mask', ...
    'MaskSource', 'Input port');

% Create a 2-D spatial reference object defining the size of the panorama.
xLimits = [xMin xMax];
yLimits = [yMin yMax];
panoramaView = imref2d([height width], xLimits, yLimits);

% Create the panorama.
for i = 1:buildingScene.Count

    I = read(buildingScene, i);

    % Transform I into the panorama.
    warpedImage = imwarp(I, tforms(i), 'OutputView', panoramaView);

    % Overlay the warpedImage onto the panorama.
    panorama = step(blender, panorama, warpedImage, warpedImage(:,:,1));
end

figure
imshow(panorama)
```

Appendix B

```
% ar_drone_ndvi.m - NDVI using AR Drone 2 modified with red and yellow filters
% HJSIII, 15.04.10

clear

% 150410 photos
fn = 'IMG_0039.JPG';  % no filter 01 - about 4 feet AGL
fn = 'IMG_0040.JPG';  % no filter 02
fn = 'IMG_0041.JPG';  % no filter 03
fn = 'IMG_0042.JPG';  % red filter 01
fn = 'IMG_0043.JPG';  % red filter 02
fn = 'IMG_0044.JPG';  % red filter 03
fn = 'IMG_0045.JPG';  % yellow filter 01
fn = 'IMG_0046.JPG';  % yellow filter 02
fn = 'IMG_0047.JPG';  % yellow filter 03

% 150416 photos
fn = 'IMG_0054.JPG';  % no filter plot A - 41 inch AGL
fn = 'IMG_0055.JPG';  % red filter plot A
fn = 'IMG_0056.JPG';  % no filter plot B
fn = 'IMG_0057.JPG';  % red filter plot B
fn = 'IMG_0058.JPG';  % red filter plot B shadow
fn = 'IMG_0059.JPG';  % no filter plot C
fn = 'IMG_0060.JPG';  % red filter plot C
fn = 'IMG_0062.JPG';  % no filter plot E sand
fn = 'IMG_0063.JPG';  % red filter plot F sand

% load image - uint8
fn = 'IMG_0057.JPG';
a = imread( fn );
[ nr, nc, nk ] = size( a );

% get lat/lon/alt from Exchangeable Image File Format
exif = imfinfo( fn );
%lat = exif.GPSInfo.GPSLatitude      % [ deg min sec ]
%lon = exif.GPSInfo.GPSLongitude     % [ deg min sec ]
%alt = exif.GPSInfo.GPSAltitude      % [ m ]
```

```
% maximum raw values
max_rgb(1) = max( max( a(:,:,1) ) );
max_rgb(2) = max( max( a(:,:,2) ) );
max_rgb(3) = max( max( a(:,:,3) ) );
max_rgb

% red filter NDVI - also yellow filter
nir = double( a(:,:,1) );  % blue pixels contain NIR
vis = double( a(:,:,3) );  % red pixels contains visible
ndvi = (nir - vis) ./ ( nir + vis );    % theoretical scaled -1 to +1, never < 0

ndvi = 2*ndvi;

% handle division by zero
ndvi( find(isnan(ndvi)) ) = 0;

% min/max/mean
min_ndvi  = min( min( ndvi ) );
max_ndvi  = max( max( ndvi ) );
mean_ndvi = mean( mean( ndvi ) );
min_max_mean_ndvi = [ min_ndvi  max_ndvi  mean_ndvi ]
```

```
% scale 0 to 255
ndvi_0_255 = uint8( 256 * ndvi );
ndvi_0_255( find( ndvi_0_255 < 0 ) ) = 0;
ndvi_0_255( find( ndvi_0_255 > 255 ) ) = 255;

% NDVI image
ndvi_rgb(:,:,1) = 255 - ndvi_0_255;
ndvi_rgb(:,:,2) = ndvi_0_255;
ndvi_rgb(:,:,3) = zeros( nr, nc, 'uint8' );

% save image as JPG
imwrite( ndvi_rgb, 'ndvi_rgb.jpg', 'jpeg' )
```

```
% show images
figure( 1 )
  clf
  subplot( 2,1,1 );
    image( a  )
    title( 'RGB' )
    axis equal
    axis( [ 1 nc  1 nr ] )
  subplot( 2,1,2 );
    image( ndvi_rgb )
    title( 'NDVI')
    axis equal
    axis( [ 1 nc  1 nr ] )

% show histogram
x = ( 0 : 0.01 : 1 );
ndvi_hist = sum( hist( ndvi, x )' );
figure( 2 )
  clf
  plot( x, ndvi_hist )
  title( 'NDVI histogram' )
  xlabel( 'NDVI' )
  ylabel( 'Count' )
```

ACADEMIC VITA

Academic Vita of Connor Disco
cdisco28@gmail.com

Education

B.A. 2016 The Pennsylvania State University Schreyer Honors College
Majors: Mechanical Engineering
Minors: Engineering Leadership Development, Engineering Mechanics

Thesis Title: Measuring Normalized Differential Vegetation Index for Agricultural Management Using Unmanned Aerial Vehicles
Thesis Supervisor: Henry Joseph Sommer III

Work Experience

Summers 2014, 2015
Westinghouse Electric Company
Engineering Intern
- Diagnosed structural safety concerns through model-development and FEA
- Aided in the construction of analytical solutions to address safety concerns
- Coded transient data for use in analytical studies
- Developed and verified structural models for power plant components

Grants Received

College of Engineering Research Experience for Undergraduates
Summer Discovery Grant

Publications

The Impact of Virtual Product Dissection on Engineering Learning and Self-Efficacy
ASME International Design Engineering Technical Conferences & Design Education